Comparison of the Deformation Microstructures at Room Temperature in O and B2 Phases of a Ti2AlNb Alloy

F. Popille, Joël Douin

JOURNAL DE PHYSIQUE IV
Colloque 2, supplément au Journal de Physique III, Volume 6, mars 1996

Comparison of the Deformation Microstructures at Room Temperature in O and B2 Phases of a Ti_2AlNb Alloy

F. Popille and J. Douin

Laboratoire d'Etude des Microstructures (UMR 104 CNRS/ONERA), 29 avenue de la Division Leclerc, BP. 72, 92322 Châtillon Cedex, France

Abstract: The dislocation microstructures in both O and B2 single phases of a Ti_2AlNb alloy, deformed at room temperature, are reported. Slip systems activated during the deformation of each phase are determined using weak-beam electron microscopy and the correspondence between the deformation processes is made. It is shown that the better ductility of the B2 phase compared to the O phase is related to the number of activated slip systems.

1. INTRODUCTION

For twenty years, research on intermetallic compounds have been of great interest to aircraft engine applications since these alloys have a low density and a high temperature strength [1]. Titanium aluminides based on Ti_3Al materials are candidates for such applications but they are handicapped by a low ductility at room temperature due to a limited number of independant slip systems available in their hexagonal close-packed structure [2,3].
The development of new Ti_3Al-based alloys with some room temperature ductility has become possible through the addition of transition elements such as Nb, Mo or V. In particular, Nb-rich titanium aluminides near the Ti_2AlNb composition have a better room temperature ductility and fracture toughness than conventional titanium aluminides [4].
The as-cast former alloys are two-phased and their microstructures consist of either precipitates of an ordered orthorhombic phase (O phase) embedded in a matrix of an ordered b.c.c phase (B2 phase) or precipitates of B2 phase within an O matrix. Appropriate heat treatments lead to the formation of single-phase alloys of either the O phase or the B2 phase.
The present study reports on the microstructure after deformation at room temperature of each phase of a Ti_2AlNb alloy. By using weak-beam transmission electron microscopy, Burgers vectors and glide systems of the dislocations activated during deformation are determined in order to compare the deformation processes of each phase.

2. EXPERIMENTAL

The $Ti_{53}Al_{25}Nb_{22}$ (at. %) alloy has been prepared under vacuum in a high frequency induction furnace. Parallelepipedic samples of dimensions 3x3x8 mm^3 were spark machined from the ingot and heat treated in order to obtain O or B2 single-phase alloys. In order to avoid oxydation during the heat treatments the samples were envelopped with Ti-Zr chips in a Nb foil. Table 1 indicates the applied heat treatments. Prior to mechanical testing, the surface irregularities were removed by mechanical polishing. Both single-phase alloys were deformed in compression at room temperature. The compression tests were carried out at a constant strain rate of 2.10^{-3} s^{-1} and stopped after 2% plastic strain to obtain a moderate dislocation density. Discs were sliced at 45° from the compression axis in order to maximize the probability that the foils contain

a slip system. The slices were then mechanically thinned to 100 μm and electropolished in a solution of 5% $HClO_4$, 35% 2-butoxyethanol and 60% methanol at 0°C under 15V. The foils were examined under a JEOL 200CX transmission electron microscope operating at 200kV. The weak-beam investigations were performed using a double-tilt holder.

B2 phase	1140°C, 1h, water quenched
O phase	1200°C, 48h, oil quenched + 900°C, 300h, oil quenched

Table 1

3. DISLOCATION MICROSTRUCTURES AFTER DEFORMATION AT ROOM TEMPERATURE

3.1 In the O phase

After deformation at room temperature, the microstructure of the O phase consists in the activation of the [100], 1/2 [110] and 1/2 [1$\bar{1}$0] dislocations (see fig. 5a). These dislocations glide in the (010), (1$\bar{1}$0) and (110) planes, respectively, where they are split into two identical superpartials separated by an antiphase boundary (APB) according to the following reactions :

$$[100] \rightarrow 1/2\,[100] + \text{APB} + 1/2\,[100] \quad (1)$$

$$1/2\,[110] \rightarrow 1/4\,[110] + \text{APB} + 1/4\,[110] \quad (2)$$

$$1/2\,[1\bar{1}0] \rightarrow 1/4\,[1\bar{1}0] + \text{APB} + 1/4\,[1\bar{1}0] \quad (3)$$

Notice that the [100], 1/2 [110] and 1/2 [1$\bar{1}$0] translations are almost equivalent and only differ by a slight change in magnitude, and that the (010), (1$\bar{1}$0) and (110) planes are also very closely related since they correspond to the first order prismatic planes of the α_2 parent structure [5,6].

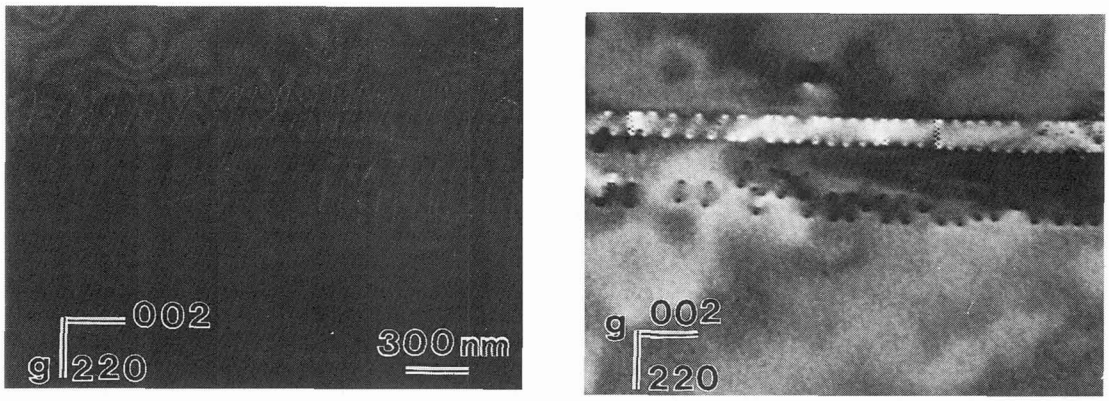

a) b)

Figure 1: Slip band of [100] dislocations formed during deformation at room temperature : a) weak-beam micrograph imaged with the Beam Direction **BD** near [$\bar{1}$10] and diffraction vector **g** = 220 ; b) **BD** near [$\bar{1}$10], **g** = 002, a residual contrast due to some relaxation occurs at the intersection of the dislocations with the foil surface.

Dislocations propagation in slip bands is typical of the deformation microstructure, as illustrated in fig. 1. In this slip band the dislocations have a Burgers vector parallel to [100] since they are out of contrast with the 021 and 002 reflections. The line direction of the segments, determined by stereographic analysis, is parallel or close to [100], that is, in screw orientation. Fig. 1b, imaged with the diffracting vector $\mathbf{g} = 002$, shows some residual contrast at the intersection of the foil surface by the dislocations. The emergence points are aligned along the [001] direction. The dislocations are thus gliding in the (010) plane. Tilting experiments and dissociation width measurements show that (010) is also their plane of dissociation.

Interactions between [100], 1/2 [110] and 1/2 [1$\bar{1}$0] dislocations have been also observed but they play a less significant role [7].

3.2 In the B2 phase

The microstructure after deformation at room temperature is characterized by a large density of <111> superdislocations in screw orientation. Slip of dislocations in the B2 phase occurs on {110} or {112} planes , where the superdislocations are split into two identical superpartials leading to an APB formation according to :

$$<111> \rightarrow 1/2 <111> + \text{APB} + 1/2 <111> \qquad (4)$$

Fig. 2 shows a typical arrangement of the dislocations.

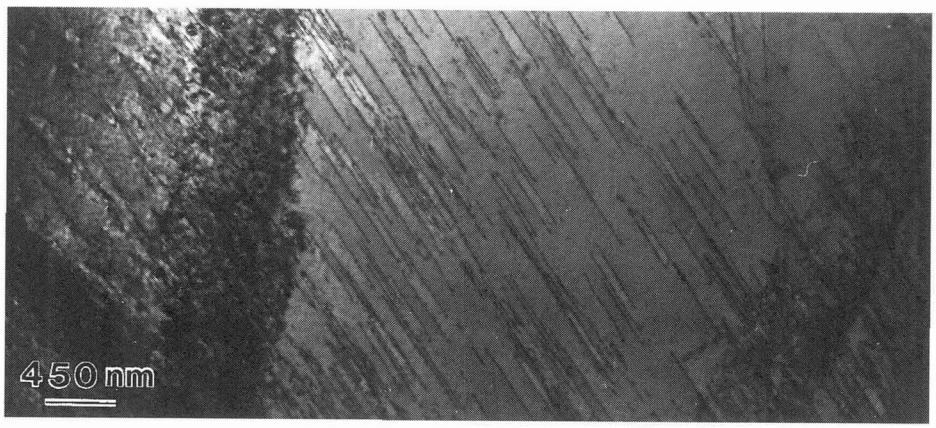

Figure 2 : <111> dislocations activated during deformation of the B2 phase at room temperature, imaged in bright field.

Dislocations on fig. 3 are out of contrast when imaged with $\mathbf{g} = 110$ and $\mathbf{g} = \bar{1}01$, their Burgers vector is therefore [1$\bar{1}$1]. The dislocation marked with the arrow in fig. 3a is shown at higher magnification in fig. 3b. Crystallographic analysis reveals that the dislocations are preferentially aligned along the [1$\bar{1}$1] and [110] directions (segments 1 and 2, respectively), confirming that ($\bar{1}$12) is their gliding plane. It is worth emphasizing that the [1$\bar{1}$1] half loop of fig. 3b adopts a shape attesting of a significant elastic anisotropy. Furthermore, the edge part of the dislocation is dissociated by climb according to reaction (4) in a plane close to (001). Note that climb of edge dislocations at room temperature in a B2 compound has been already reported in β-CuZn [8].

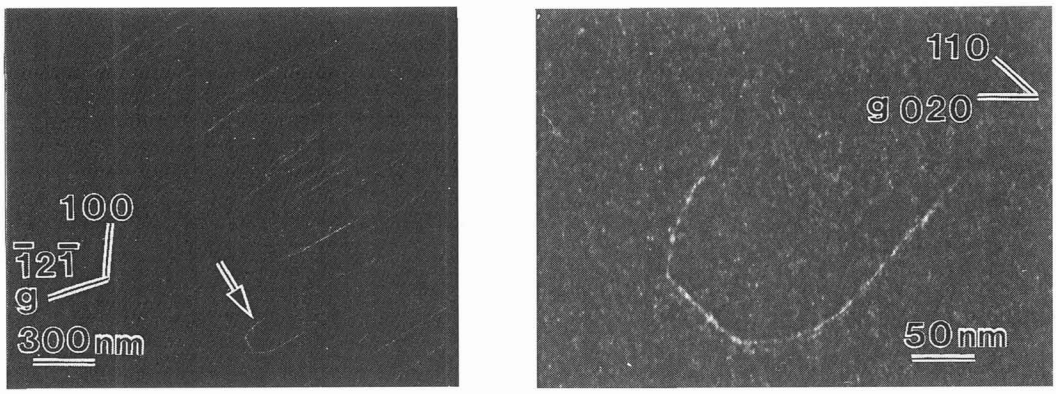

a) b)

Figure 3 : Glissile $[1\bar{1}1]$ dislocations formed in the B2 phase after deformation at room temperature: a) weak-beam (WB) micrograph recorded with **BD** near $[0\bar{1}2]$ and **g** = $\bar{1}2\bar{1}$: the arrow identifies the dislocation mentionned in the text ; b) Higher magnification WB micrograph imaged with **BD** near $[00\bar{1}]$ and **g** = 020: note the particular shape of the dislocation loop attesting a significant elastic anisotropy.

Observations of scalloped dislocations between slip bands is also a common feature of the deformation microstructure of the B2 phase. The APB width variation between the two 1/2<111> superpartials, shown in fig. 4a, results from a strong pinning and attests of a sessile configuration. A local variation of the composition might be responsible for this pinning and can be associated with the streaking and diffuse intensity shown up on fig. 4b. Such a lattice instability gives rise to the tweed contrast, i.e. the continuous background modulation, which is observed for many diffracting conditions in this alloy (fig. 4b). As the B2 phase is metastable, it is believed that O phase precipitation is at the origin of the lattice inhomogeneity.

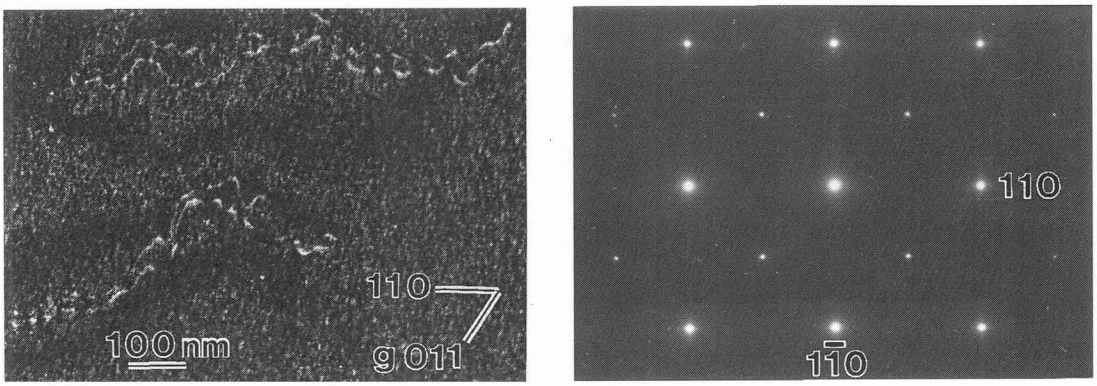

a) b)

Figure 4 : Influence of a local variation of the composition : a) strongly pinned dislocations in a sessile configuration, imaged with **BD** near $[\bar{1}1\bar{1}]$ and **g** = 011 ; b) selected area diffraction pattern with **BD** near $[00\bar{1}]$ showing diffuse intensity line along the <110>* directions.

3.3 Planar defect energies estimate

The energies of planar defects are found by calculating the repulsive force between partial dislocations at equilibrium. Although both phases exhibit a non negligeable anisotropy, since the elastic constants are unknown isotropic elasticity has been assumed. A Poisson's coefficient of $\nu = 1/3$ has been used and the

shear moduli, determined from the deformation curves are $\mu_O = 5.10^4$ MPa and $\mu_{B2} = 4.4.10^4$ MPa. The results of the calculations are listed in table 2.

	Burgers vector	dissociation plane	dissociation width (nm)	estimated APB energy (mJ/m^2)
O	[100]	(010)	8.4 ± 1	85 ± 10
B2	[111]	(001)	3.7 ± 1	150 ± 50

Table 2

4. COMPARISON OF DEFORMATION MODE

The O phase is structurally closely related to the Ti_3Al (α_2) ordered hexagonal structure with a lattice distortion resulting from an excess of Nb atoms in the α_2 lattice [5,6]. There is also a lattice correspondence between O and B2 structures, similar to what exists between O and b.c.c. phases [9,10], exemplified in figure 5:

$$\mathbf{a}_O/2 = 1/2[100]_O \approx [001]_{B2},$$
$$\mathbf{b}_O/2 = 1/2[010]_O \approx [1\bar{1}0]_{B2},$$
$$\mathbf{c}_O = [001]_O \approx [110]_{B2}$$

with mismatches -6.6%, +3.8% and +1.7%, respectively. These relationships lead to:

$$1/2[1\bar{1}0]_O \approx [1\bar{1}1]_{B2}$$
$$1/2[1\bar{1}0]_O \approx [\bar{1}11]_{B2}$$

In the same vein, the arrangement of atoms in the (001) plane of the O structure is similar to the one in the (110) plane of the B2 structure, both being the densest plane in each phase (fig.5). The (110) and $(1\bar{1}0)$ planes of the O structure are also closely related to the {112} planes of the B2 structure: for example in the case of the lattice correspondence in fig.5, $(110)_O \approx (1\bar{1}2)_{B2}$ and $(1\bar{1}0)_O \approx (\bar{1}12)_{B2}$.

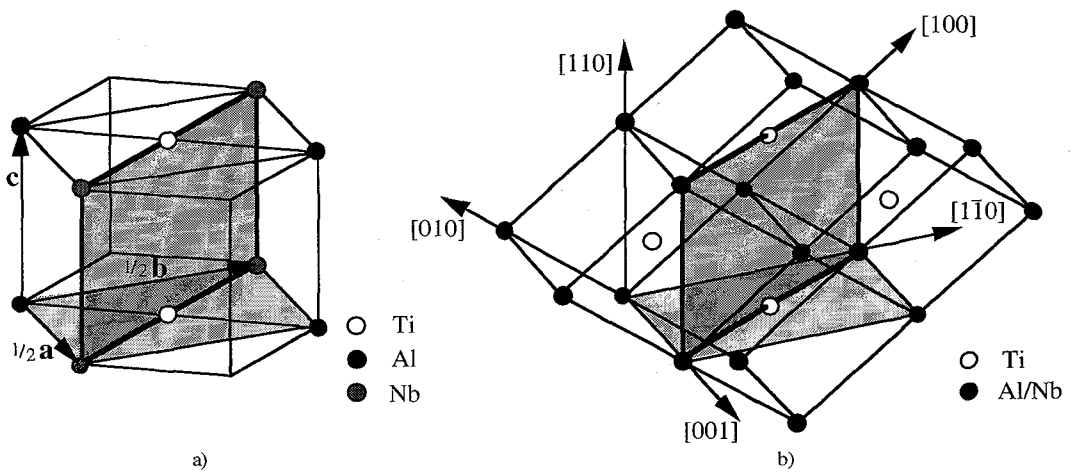

Figure 5 : Correspondence between O and B2 structures. a) O phase: for sake of clarity, only one-fourth of the unit cell and atoms of the (001) plane have been drawn ; b) arrangement of B2 unit cells.
The lattice parameters, deduced from selected area diffraction patterns are $a_O = 0.60 \pm 0.01$ nm, $b_O = 0.94 \pm 0.02$ nm, $c_O = 0.46 \pm 0.01$ nm and $a_{B2} = 0.32 \pm 0.03$ nm. Planes $(001)_O$ and $(110)_O$ of the O phase corresponding to $(110)_{B2}$ and $(1\bar{1}2)_{B2}$ planes of the B2 structure, respectively, have been shouded.

In the O phase, [100], 1/2 [110] and 1/2 [1$\bar{1}$0] dislocations glide in slip bands on (010), (1$\bar{1}$0) and (110) planes, respectively, while in the B2 phase, rectilinear screw dislocations with <111> Burgers vectors glide on {$\bar{1}$12} and {110} planes. According to the above correspondence, in a first approximation slip systems 1/2[110](1$\bar{1}$0)$_O$ and 1/2[1$\bar{1}$0](110)$_O$ in the O phase are equivalent to slip systems [1$\bar{1}$1]($\bar{1}$12)$_{B2}$ and [$\bar{1}$11](1$\bar{1}$2)$_{B2}$ of the B2 phase, respectively. The correspondence holds true for [100](010)$_O$ and [002](1$\bar{1}$0)$_{B2}$. Thus, the deformation in the two phases appears to occur in very similar ways. What differs is the number of possible activated slip systems in each structure: there only exist three activated slip systems in the O phase, namely 1/2[110](1$\bar{1}$0)$_O$, 1/2[1$\bar{1}$0](110)$_O$ and [100](010)$_O$, while twelve slip systems of the <111>{112}$_{B2}$ type and three of the <111>{011}$_{B2}$ type can be activated in the B2 alloy. This explain why the B2 alloy can attain a better room temperature ductility [11], than the alloy with the O structure, in the same range of composition and temperature, especially when deformed in tension [6].

The correspondence of the slip systems in the two phases has another consequence. In a two-phased alloy, what would help transmission of the deformation though the material is the ability for dislocations to be not very much disturbed at the passage through a B2/O interface. It is thus believed that the correspondence between the slip systems favors the transmission of the deformation from one phase to the other, thus gives rise to an explanation of the rather good ductility at room temperature of the two-phased alloys [4].

Acknowledgments

F.P. is grateful to the Direction des Recherches, Etudes et Techniques (DRET) for the provision of a Ph.D. research fellowship.

References

[1] Larsen J.M., Williams A., Balsone S.J. and Stucke M.A., *High Temperature Aluminides and Intermetallics* (edited by S.H. Wang, C.T. Liu, D.P. Pope and J.O. Stiegler, Warrendale, PA: TMS, 1990), p.251.
[2] Lipsitt H.A., Shectman D. and Shafrik R.E., *Metall. Trans.* A **11** (1980) 1369.
[3] Lipsitt H.A., *High Temperature Ordered Intermetallic Alloys* (edited by C.C Koch, C.T. Liu and N.S.Stoloff, Pittsburgh, PA: MRS, 1985) p.351.
[4] Rowe R.G., Konitzer D.G., Woodfield A.P. and Chesnutt J.C., *High Temperature Ordered Intermetallic Alloys* (edited by L.A. Johnson, D.P. Pope and J.O. Stiegler, Pittsburgh, PA: MRS, 1991) p.703.
[5] Hsiung L. M. and Wadley H. N. G. , *Scripta. Met.* **27** (1992) 605.
[6] Banerjee D. , Gogia A. K. , Nandy T. K. and Joshi V. A. , *Acta. Met* **36** (1988) 871.
[7] Popille F. and Douin J., submitted to *Phil. Mag. A.*
[8] Dirras G., Beauchamp P. and Veyssière P., *Phil. Mag. A* **65** (1992) 815.
[9] Bendersky L. A. ,Boettinger W. J. and Roytburd A. , *Acta. metall. mater.* **39** (1991) 1959.
[10] Bagaryatskii I.A., Nosova G.I. and Tagunova T.V., *Soviet Phys. Dokl.* **3** (1959) 914.
[11] Naka S., Thomas M., Marty M., Lapasset G. and Khan T., *Structural Intermetallics* (edited by R. Darolia, J.J. Lewandowski, C.T. Liu, P.L. Martin, D.B. Miracle and H.V. Nathal, Warrendale, PA: TMS, 1993), p.647.